

Radiative proton capture on ^{15}N within effective field theory

Sangyeon Son,^{1,*} Shung-Ichi Ando,^{2,†} and Yongseok Oh^{1,3,‡}

¹*Department of Physics, Kyungpook National University, Daegu 41566, Korea*

²*Department of Display and Semiconductor Engineering, Sunmoon University, Asan, Chungnam 31460, Korea*

³*Asia Pacific Center for Theoretical Physics, Pohang, Gyeongbuk 37673, Korea*

The astrophysical S factor for the radiative proton capture process on the ^{15}N nucleus, i.e., $^{15}\text{N}(p, \gamma)^{16}\text{O}$, at stellar energies are studied within the framework of the cluster effective field theory. The thermonuclear $^{15}\text{N}(p, \gamma)^{16}\text{O}$ reaction links the type-I to type-II cycles of the carbon-nitrogen-oxygen cycle and affects the abundances of elements in the universe. For investigating this reaction in the effective field theory formalism, we first construct an effective Lagrangian that is appropriate for this reaction at low-energies. Since the intermediate excited states of the ^{16}O nucleus have a crucial role in this reaction, we include these resonances in the formalism. The corresponding radiative capture amplitudes and cross section are calculated, which lead to the astrophysical S factor. The low energy constants introduced in the effective Lagrangian are determined by fitting the theoretical results to the observed S factors in the range of $130 \text{ keV} < E_p < 2500 \text{ keV}$ using three different experimental data sets. Considering the recent data sets, we obtain $S(0) = 29.8\text{--}34.1 \text{ keV b}$, which is in a good agreement with the estimates from R -matrix approaches in the literature. The values of S at the Gamow energy are found to be larger than $S(0)$ values by about 10%.

I. INTRODUCTION

Thermonuclear fusion is the energy source of stars. Among thermonuclear fusion processes, the proton-proton chain and the carbon-nitrogen-oxygen (CNO) cycle are two major processes [1, 2]. The neutrinos produced in the Sun by these processes have been observed in underground experiments [3–6], which brings information on the solar neutrinos and confirmed the thermonuclear reactions of the proton-proton chain and the CNO cycle inside the Sun. In the CNO cycle, the proton capture reaction on ^{15}N allows two possible channels, namely, $^{15}\text{N}(p, \alpha)^{12}\text{C}$ and $^{15}\text{N}(p, \gamma)^{16}\text{O}$. The former is responsible for the type-I cycle (CN cycle) and the latter for the type-II cycle (NO cycle). At low energies the CN cycle is dominant but at higher temperatures the NO cycle becomes active. Since the CN and NO cycles intersect at the nucleus ^{15}N , the relative strength of the two reactions, $^{15}\text{N}(p, \alpha)^{12}\text{C}$ and $^{15}\text{N}(p, \gamma)^{16}\text{O}$, determines the probability of the path in the CNO cycle. It turns out that the rate for the former reaction is much larger than for the latter, which means that the CN cycle is more probable than the NO cycle. Although its contribution to the energy production in stars would be small, the $^{15}\text{N}(p, \gamma)^{16}\text{O}$ reaction is crucial to understand nucleosynthesis and the observed oxygen abundances. Therefore, the evaluation of its cross sections at stellar energy scales is strongly required for resolving such issues [7, 8].

Because of the Coulomb barrier, the nuclear reaction cross section $\sigma(E)$ at the center-of-mass (c.m.) energy E is parameterized by the astrophysical S factor defined as

$$S(E) = E\sigma(E)\exp(2\pi\eta), \quad (1)$$

where η is the dimensionless Sommerfeld parameter,

$$\eta = Z_A Z_B \mu \alpha_{\text{em}} / p \quad (2)$$

with the fine structure constant $\alpha_{\text{em}} = e^2/(4\pi)$. Here, μ is the reduced mass of the system, $\mu \equiv m_A m_B / (m_A + m_B)$, where m_A and m_B are the masses of the initial state nuclei whose charges are Z_A and Z_B , respectively. The magnitude of the relative spatial momentum between the two nuclei in the c.m. frame is represented by p .

Thus the astrophysical S factor is the main characteristic of any thermonuclear reaction at low energies. Determination of its value by experiments is, however, highly nontrivial as the most experiments are carried out at the energies above 100 keV, while the realistic energy scale for astrophysical environments is about 0.1–100 keV. Thus, we need the value of $S(0)$ in practical calculations as $S(E)$ is a very slowly varying function of energy at low energy region.¹ Therefore, most realistic method for obtaining the astrophysical S factor at zero energy would be the extrapolation of experimentally determined $S(E)$ to the lower energy range. However, because of the difficulties of experiments near threshold, larger error bars at low energy region are inevitable and this causes the uncertainties of $S(0)$. The extrapolation would, of course, depend on the theoretical models adopted for the description of the reaction.

Despite the importance of the $^{15}\text{N}(p, \gamma)^{16}\text{O}$ reaction, experimental measurements of its cross sections at low energies are rare and only two measurements were reported until 2009 [10, 11].² The first measurement was made about 60 years ago [10], which was then followed by the work of Ref. [11] in mid 1970s. The former experiment reported $S(0) \approx 32 \text{ keV b}$, while the latter estimated $S(0) = 64 \pm 6 \text{ keV b}$. This shows that the value of the latter experiment is about twice that of the former one. However, these experiments

¹ The cold and hot CNO burning cycles have the Gamow peak energy regions at $E_G \approx 26 \text{ keV}$ and $150\text{--}200 \text{ keV}$ for the corresponding core temperatures at $T_c \approx 1.5 \times 10^7 \text{ K}$ and $(2\text{--}3) \times 10^8 \text{ K}$, respectively [7, 9].

² The experimental data reported in Ref. [12] are for $E_p \geq 860 \text{ keV}$ and do not constrain the value of $S(0)$, where E_p is the kinetic energy of the incident proton in the laboratory frame. We also note that the data of Ref. [13] covered the region of $E_p > 250 \text{ keV}$.

* thstkd3754@gmail.com

† sando@sunmoon.ac.kr

‡ yohphy@knu.ac.kr

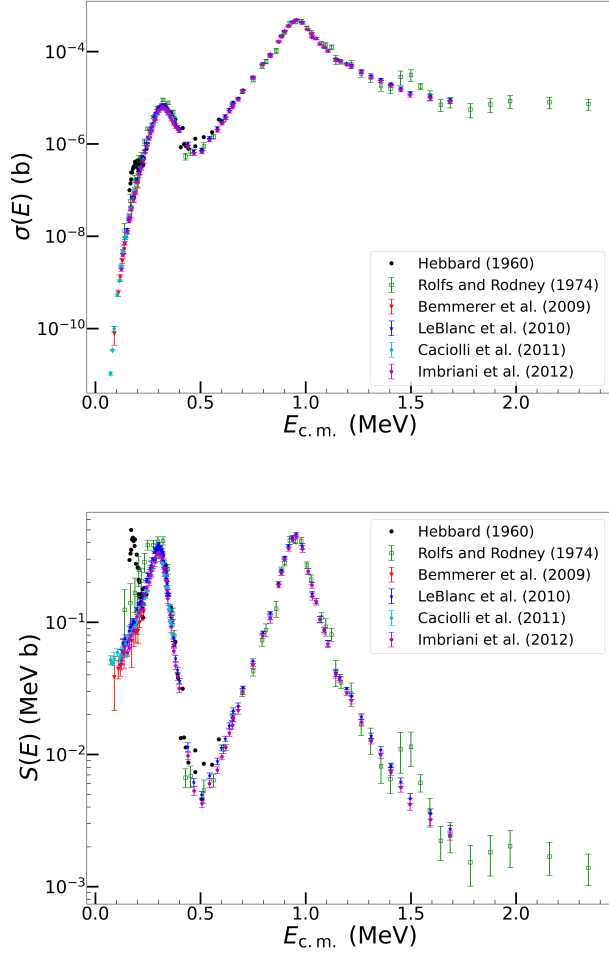


FIG. 1. Collected experimental data for (a) the cross sections and (b) the astrophysical S factors $S(E)$ of the $^{15}\text{N}(p, \gamma)^{16}\text{O}$ reaction. The data from Refs. [10, 11, 17–19, 25] are compiled in Ref. [23].

verified that the reaction is dominated by the first two interfering $J^\pi = 1^-$ resonances at $E_R = 312$ and 964 keV, respectively, where E_R is the resonance energy in the center-of-mass frame [14].³ These two data sets are used for the analyses in Refs. [14–16]. In particular, it was pointed out in Ref. [14] that the contribution from the direct capture process was overestimated in Ref. [11].

In the last decade, more measurements were performed at the Laboratory for Underground Nuclear Astrophysics (LUNA) at Gran Sasso underground laboratory (LNGS) and at the Notre Dame Nuclear Science Laboratory [17–19]. These efforts are summarized in Refs. [20, 21] and the data are collected, for example, in Refs. [22, 23] which are used for updating the estimation of the S factors in Refs. [24–27].⁴ The

newly estimated values of $S(0)$ based on these data sets, called the post-NACRE data, are as low as 33.1 keV b [24] and as high as 45^{+9}_{-7} keV b [22].

Shown in Fig. 1 are currently available experimental data of $^{15}\text{N}(p, \gamma)^{16}\text{O}$ compiled in Ref. [23]. Figure 1(a) shows the total cross section data, while Fig. 1(b) presents the derived astrophysical S factors. They are given as functions of E_{cm} , the kinetic energy of the system in the center-of-mass frame. These figures explicitly show that the reaction is dominated by the two broad resonances mentioned previously. Except the earlier data of Refs. [10, 11], the reported data show a good agreement. The cross section data of Ref. [10] indicate a small structure at very low energies and it is further exaggerated in the astrophysical S factor as shown by black dots in Fig. 1(b). It is also evident that the data of Ref. [11] have larger error bars compared with the data of the next generation experiments. Furthermore, the data from Ref. [17, 19] do not cover the second resonance region. Therefore, in the present work, we focus on the data covering the both resonance regions, which include the data of Ref. [11] and the post-NACRE data of Refs. [18, 25], and apply our calculations to these three experimental data sets.

In the present work, we apply the effective field theory (EFT) formalism to investigate the $^{15}\text{N}(p, \gamma)^{16}\text{O}$ reaction. EFTs allow for a systematic calculation by introducing a scale Λ_H which separates relevant degrees of freedom at low energies from irrelevant degrees of freedom at high energies. Then the effective Lagrangian is constructed by the expansion with the number of derivatives, and the reaction amplitudes are calculated in powers of Q/Λ_H where Q is a typical momentum scale of the reaction in question. The irrelevant high energy degrees of freedom are integrated out and the coefficients in the effective Lagrangian, called low-energy constants (LECs), are determined by fitting the experimental data [28]. EFT methods have been applied to the studies of various reactions including thermonuclear reactions such as α capture on ^{12}C [29], radiative proton capture on ^{12}C [30], and proton and neutron capture on light nuclei [31–35]. It was also applied to the reactions of ^{15}C [36], α - ^{12}C elastic scattering [37–39], and β delayed α emission from ^{16}N [40], and so on. Reviews on these topics can be found, for example, in Refs. [41–44].

The construction of EFT for the $^{15}\text{N}(p, \gamma)^{16}\text{O}$ reaction involves three open channels, namely, p - ^{15}N , α - ^{12}C , and α - $^{12}\text{C}^*$ where $^{12}\text{C}^*$ denotes the first excited 2^+ state of ^{12}C . In the present study, by focusing on the $^{15}\text{N}(p, \gamma)^{16}\text{O}$ reaction data, we perform the single channel calculations leaving the coupled-channel calculations to a future work. The energy range of the data of our interests covers up to $E \simeq 2$ MeV, which includes the aforementioned two s -wave resonant states of ^{16}O . The inclusion of a resonant state in EFT was investigated, for example, by Gelman [45] and by Habashi, Fleming, and van Kolck [46], and, following their method, we here employ the effective Lagrangian for the p - ^{15}N system with the two resonant states of ^{16}O .

³ The corresponding excitation energies are 12.45 MeV and 13.09 MeV, respectively. In the laboratory frame, these values correspond to $E_p = 338$ keV and 1028 keV, respectively.

⁴ The experimental data of Ref. [18] are compiled in Ref. [26]. In the present

work, we use the experimental data compiled in Experimental Nuclear Reaction Data (EXFOR) [23].

We choose the breakup energy of ^{16}O into the n - ^{15}O channel, $\Delta E = 3.54$ MeV, as the large energy scale, which gives $\Lambda_H = \sqrt{2\mu\Delta E} = 80$ MeV, where μ is the reduced mass of the system. On the other hand, the resonant energies, $E_1 = 0.312$ MeV and $E_2 = 0.964$ MeV, are chosen as the typical energy scales of the theory leading to $Q_1 = \sqrt{2\mu E_1} = 24$ MeV and $Q_2 = \sqrt{2\mu E_2} = 41$ MeV. Therefore, our expansion parameters are $Q_1/\Lambda_H \simeq 0.3$ and $Q_2/\Lambda_H \simeq 0.5$, and the terms in the amplitudes are expanded in powers of $(Q_{1,2}/\Lambda)^{2n}$ as the effective range expansion (ERE). We include the terms up to the next-to-leading order for the first resonant state and up to the fourth order terms for the second so that the theoretical uncertainties of the present calculations are estimated as $(Q_1/\Lambda_H)^2 \simeq 0.09$ and $(Q_2/\Lambda_H)^6 \simeq 0.016$.

Our preliminary results in this approach were reported in Ref. [47] where only the first resonance was considered with the experimental data of Ref. [19]. The estimated astrophysical S factor is $S(0) = 30.4$ keV b that is close to the lower limit of $S(0)$ obtained in the recent analyses of Ref. [24]. In the present work, we perform more complete analysis working with the data covering the energy regions of both resonances which were reported in Refs. [11, 18, 25].

This paper is organized as follows. In the next section, we develop the cluster EFT formalism for the reaction of

$^{15}\text{N}(p, \gamma)^{16}\text{O}$ by introducing the effective Lagrangian for this reaction. In Sec. III, the propagator of the di-field, which is introduced for the description of resonances, is discussed. Then the capture amplitudes are derived in Sec. IV, and Sec. V presents our numerical results which are compared with the estimates in the literature. Section VI summarizes this work and the derivation of the loop integral formulas is given in Appendix.

II. EFFECTIVE LAGRANGIAN

The cluster EFT, which is applied to the investigation of nuclear reactions at stellar environments, is similar to the pionless EFT [48, 49] by adopting contact couplings among the participating particles. In the present approach, we treat the nuclei involved in the reaction of $^{15}\text{N}(p, \gamma)^{16}\text{O}$ as point-like particles, and describe resonance states $^{16}\text{O}^*$ as bound systems of the proton and the ^{15}N nucleus. The high energy scale is determined by the breakup energy of ^{16}O and the resonant energies are used to estimate the low energy scales.⁵

Since we have two resonant $^{16}\text{O}^*$, we construct the effective Lagrangian for this reaction as

$$\begin{aligned} \mathcal{L} = & \psi_p^\dagger \left\{ i v \cdot D + \frac{1}{2M_p} [(v \cdot D)^2 - D^2] \right\} \psi_p + \psi_N^\dagger \left\{ i v \cdot D + \frac{1}{2M_N} [(v \cdot D)^2 - D^2] \right\} \psi_N \\ & + \sum_{n=0}^{n_{\max}} C_n^{(I=0)} d_i^{(I=0)\dagger} \left\{ i v \cdot D + \frac{1}{2(M_p + M_N)} [(v \cdot D)^2 - D^2] \right\}^n d_i^{(I=0)} \\ & + \sum_{m=0}^{m_{\max}} C_m^{(I=1)} d_{ia}^{(I=1)\dagger} \left\{ i v \cdot D + \frac{1}{2(M_p + M_N)} [(v \cdot D)^2 - D^2] \right\}^m d_{ia}^{(I=1)} \\ & - y_t^{(I=0)} \left\{ d_i^{(I=0)\dagger} \left(\psi_p^T P_i^{(3S_1)} \psi_N \right) + \text{H.c.} \right\} - y_t^{(I=1)} \left\{ d_{ia}^{(I=1)\dagger} \left(\psi_p^T P_{ia}^{(3S_1)} \psi_N \right) + \text{H.c.} \right\} \\ & - y_s \left\{ \phi_O^\dagger \left(\psi_p^T P^{(3P_0)} \psi_N \right) + \text{H.c.} \right\} - y_t^{(I=0)} h^{(I=0)} \left\{ \phi_O^\dagger (-i D_i) d_i^{(I=0)} + \text{H.c.} \right\} \\ & - y_t^{(I=1)} h^{(I=1)} \left\{ \phi_O^\dagger (-i D_i) d_{ia}^{(I=1)} \delta_{a3} + \text{H.c.} \right\}, \end{aligned} \quad (3)$$

where ψ_p , ψ_N , and ϕ_O are the fields of the proton, ^{15}N , and the ground state of ^{16}O , respectively, and the masses of the proton and ^{15}N are denoted by M_p and M_N , respectively. The interactions with higher derivatives are suppressed in the effective Lagrangian of Eq. (3). The di-fields $d^{(I=0)}$ and $d^{(I=1)}$ are introduced as auxiliary fields to describe the first and second resonance states of ^{16}O , respectively, where I in the super-

script indicates its isospin quantum number. The coupling constants y_s , $y_t^{(I)}$, and $h^{(I)}$ are the LECs which determine the strength of the contact interactions among the proton, ^{15}N , and ^{16}O nucleus.

⁵ The momentum scale corresponding to the radius of ^{16}O is about 70 MeV which is larger than our typical scales and is comparable to the large scale. The finite-range effects would be investigated by the expansion in powers of spatial derivatives.

The four-velocity vector v^μ is chosen to be $v^\mu = (1, \mathbf{0})$, and $D_\mu = \partial_\mu + ie\hat{Q}A_\mu$ is the covariant derivative where e , \hat{Q} , and A_μ are the elementary charge, charge operator, and the photon field, respectively. The projection operators in the interaction



FIG. 2. Fully-dressed propagator of the di-field. In the right hand side, the double line stands for the bare propagator and the shaded region represents the Coulomb interaction between two nuclei.

terms are defined as

$$P_i^{(^3S_1)} = \frac{1}{2} \sigma_2 \sigma_i \tau_2, \quad P_{ia}^{(^3S_1)} = \frac{1}{2} \sigma_2 \sigma_i \tau_2 \tau_a, \quad (4)$$

$$P^{(^3P_0)} = \frac{1}{2} \left(\tau_2 \sigma_2 \vec{\sigma} \cdot \frac{(-i\vec{D})}{M_N} - \frac{(-i\vec{D})}{M_p} \cdot \tau_2 \sigma_2 \vec{\sigma} \right), \quad (5)$$

where the superscript in the projection operator stands for the orbital angular momentum of the interaction between the proton and the ^{15}N nucleus. Here, σ_i are the Pauli spin matrices and τ_i are the Pauli isospin matrices. The integers n_{\max} and m_{\max} are the numbers of the considered effective range parameters of the effective range expansion (ERE) which determine the coefficients $C_n^{(I=0)}$ and $C_m^{(I=1)}$ for the iso-singlet and iso-triplet di-fields, respectively. For the two resonances these integers are chosen by $n_{\max} = 1$ and $m_{\max} = 3$ corresponding to the terms up to the second and the fourth order.⁶

III. DI-FIELD PROPAGATOR

In the present work, we depict the intermediate resonance states by considering the fully-dressed propagator of di-field $d^{(I)}$. As shown in Fig. 2, the fully-dressed propagator is expressed as an infinite series of the bare propagator D_0 and the self-energy Σ as

$$D = (D_0^{-1} - \Sigma)^{-1}. \quad (6)$$

In this figure, the self-energy is represented by the bubble diagram with a shaded region between the two bare propagators. From the Lagrangian (3), the bare propagator for $d^{(I)}$ is written as

$$D_0^{(I)}(p) = \frac{1}{C_0^{(I)} + C_1^{(I)} p^2 + C_2^{(I)} p^4 + \dots}, \quad (7)$$

where p is the magnitude of the relative spatial momentum between the two nuclei in the c.m. frame. Following the approach of Refs. [50, 51], the Coulomb interactions between the two nuclei at low-energies are described by using the Coulomb

Green's function $G_C(E)$, which leads to

$$\begin{aligned} \Sigma_{ij}(E) &= \frac{1}{2} \left(y_t^{(I)} \right)^2 \langle 0 | G_C(E) | 0 \rangle \delta_{ij} \\ &= \frac{1}{2} \left(y_t^{(I)} \right)^2 \left(-\frac{\mu}{\pi} \kappa H(\eta) + J_0^{\text{div}} \right) \delta_{ij}, \end{aligned} \quad (8)$$

where $E = p^2/2\mu$ is the total kinetic energy and

$$H(\eta) = \psi(i\eta) - \ln(i\eta) - \frac{i}{2\eta}, \quad (9)$$

where $\psi(z)$ is the digamma function defined as $\psi(z) = d[\ln \Gamma(z)]/dz$ with $\Gamma(z)$ being the gamma function. The Sommerfeld parameter η is defined as $\eta = \kappa/p$ with $\kappa = Z_p Z_N \mu \alpha_{\text{em}}$, where Z_A is the charge number of nucleus A . In our case, $\kappa = 44.9$ MeV.

The divergent part J_0^{div} arising from the Coulomb Green's function reads

$$J_0^{\text{div}} = \frac{\mu}{\pi} \kappa \left(\frac{1}{\epsilon} + \ln \frac{\Lambda \sqrt{\pi}}{2\kappa} + 1 - \frac{3}{2} \gamma_E - \frac{\Lambda}{2\kappa} \right), \quad (10)$$

where γ_E is the Euler's constant and Λ is the regularization scale introduced by performing the dimensional regularization in space-time dimension of $d = 4 - \epsilon$. The term linear in Λ comes from the power divergence subtraction scheme [52]. One may write the fully-dressed propagator by making use of the ERE so that the coefficients $C_i^{(I)}$ can be fixed by the effective range parameters [53], which gives

$$D^{(I)}(p) = - \left(y_t^{(I)} \right)^{-2} \frac{4\pi}{\mu} \frac{1}{K^{(I)}(p) - 2\kappa H(\eta)}, \quad (11)$$

and the ERE allows to write

$$K^{(I)}(p) = -\frac{1}{a_R^{(I)}} + \frac{1}{2} r^{(I)} p^2 - \frac{1}{4} P^{(I)} p^4 + \dots, \quad (12)$$

where $a_R^{(I)}$, $r^{(I)}$, and $P^{(I)}$ are the scattering length, effective range, and the shape parameter, respectively, and the divergent part J_0^{div} of Eq. (10) is absorbed by the scattering length.

Following Ref. [54], the effective range parameters appearing in the intermediate propagator are related to the resonance energy and its decay width. It is achieved by comparing the obtained amplitude of the elastic scattering process with the one obtained with the Breit-Wigner form. In Refs. [39, 55], it is modified by including additional terms in the denominator of the propagator as a result of expanding the denominator near the resonance energy. The real part of the denominator of the propagator is then expanded as

$$\begin{aligned} \tilde{K}^{(I)} &= K^{(I)} - 2\kappa \text{Re} H(\eta) \\ &= -\frac{1}{a_R^{(I)}} + \frac{1}{2} \tilde{r}^{(I)} p^2 - \frac{1}{4} \tilde{P}^{(I)} p^4 + \tilde{Q}^{(I)} p^6 \end{aligned} \quad (13)$$

⁶ As we mentioned, the orders associated with the two resonances differ. In order to further exploit the uncertainty control, we have increased the order with the lower resonance to $(Q_1/\Lambda_H)^4$ so that the theoretical uncertainties from the two resonances are similar, namely, 0.008 and 0.016, respectively. However, we could not find any improvement with this choice and we have a feature of over-fitting. Through these trials, we found that ($n_{\max} = 1$, $m_{\max} = 3$) is the optimal choice.

up to $O(p^6)$, where⁷

$$\begin{aligned}\tilde{r}^{(I)} &= r^{(I)} - 1/3\kappa, \\ \tilde{P}^{(I)} &= P^{(I)} + 1/15\kappa^3, \\ \tilde{Q}^{(I)} &= Q^{(I)} - 1/126\kappa^5.\end{aligned}\quad (14)$$

Here, the term containing κ comes from the Coulomb self-energy, $-2\kappa H(\eta)$. The imaginary part of the propagator is $-2\kappa \text{Im}[H(\eta)] = -pC_\eta^2$, where

$$C_\eta = \sqrt{\frac{2\pi\eta}{e^{2\pi\eta} - 1}} \quad (15)$$

is the Gamow factor.

Considering up to the order of p^6 in the ERE, the real part of the denominator of propagators can be expanded around the resonance energy as

$$\tilde{K}^{(I)}(E) = \sum_{n=0}^3 \frac{1}{n!} \frac{\partial^n \tilde{K}^{(I)}}{\partial E^n} \Big|_{E=E_R} (E - E_R)^n, \quad (16)$$

with $\tilde{K}^{(I)}(E_R) = 0$ where E_R is the resonance energy with $p_R = \sqrt{2\mu E_R}$. The di-field propagator with the effective range parameters can also be represented in terms of the resonance energy and width as the Breit-Wigner formula, which reads

$$D(p) = \left(y_t^{(I)}\right)^{-2} \frac{4\pi}{\mu p} \frac{\frac{1}{2}\Gamma_R(E)C_\eta^{-2}}{E - E_R + R(E) + i\frac{1}{2}\Gamma_R(E)}, \quad (17)$$

with $\eta_R = \kappa/p_R$, and the energy dependence of the resonance width is written as

$$\begin{aligned}\Gamma_R(E) &= -\frac{4\pi\kappa}{\mu(\tilde{r} - \tilde{P}p_R^2 + 6\tilde{Q}p_R^4)} \frac{1}{e^{2\pi\eta} - 1} \\ &= \Gamma_R(E_R) \frac{e^{2\pi\eta_R} - 1}{e^{2\pi\eta} - 1}.\end{aligned}\quad (18)$$

In Eq. (17), $R(E)$ contains the higher order corrections in the expansion around the resonance energy, which reads

$$R(E) = a(E - E_R)^2 + b(E - E_R)^3, \quad (19)$$

where

$$a = \frac{-\mu\tilde{P} + 12\mu\tilde{Q}p_R^2}{\tilde{r} - \tilde{P}p_R^2 + 6\tilde{Q}p_R^4}, \quad b = \frac{8\mu^2\tilde{Q}}{\tilde{r} - \tilde{P}p_R^2 + 6\tilde{Q}p_R^4}. \quad (20)$$

Through Eqs. (17)–(20) we omit isospin index I for simplicity. We take the resonance energy, width, a , and b as free parameters to be fixed by fitting the experimental data of the astrophysical S factors, which will then give the effective range parameters through Eqs. (13), (18), (20), and the condition that $\tilde{K}(E_R) = 0$.

IV. CAPTURE AMPLITUDES

The diagrams of the radiative capture amplitudes for the $^{15}\text{N}(p, \gamma)^{16}\text{O}$ reaction are depicted in Fig. 3. The capture amplitude \mathcal{M} can be decomposed into the iso-singlet and iso-triplet parts as

$$\mathcal{M} = \frac{e}{2} \chi_p^T \sigma_2 (\epsilon_\gamma^* \cdot \sigma) \tau_2 \left(X^{(I=0)} - \tau_3 X^{(I=1)} \right) \chi_N, \quad (21)$$

where the spinors for the proton and the ^{15}N nucleus in the initial state are represented by χ_p and χ_N , respectively, and ϵ_γ is the photon polarization vector. In Fig. 3, the shaded blobs represent the Coulomb repulsion between the proton and ^{15}N . The circle with a cross (\otimes) in Fig. 3(g) is the photon coupling between ^{16}O and the di-fields which is introduced as a counterterm of the loop diagrams. The isospin-dependent terms can be written as

$$X^{(I=0)} = X_{(a+b)} + X_{(c)} + X_{(d+e)}^{(I=0)} + X_{(f)}^{(I=0)} + X_{(g)}^{(I=0)}, \quad (22)$$

$$X^{(I=1)} = X_{(d+e)}^{(I=1)} + X_{(f)}^{(I=1)} + X_{(g)}^{(I=1)}, \quad (23)$$

where the amplitudes, $X_{(a,b,c)}$, $X_{(d,e,f)}^{(I=0)}$, and $X_{(d,e,f)}^{(I=1)}$ are calculated from the corresponding Feynman diagrams in Fig. 3.

In order to obtain the radiative capture amplitudes, we follow the approach advocated by the authors of Refs. [56, 57]. Using the effective Lagrangian of Eq. (3), the amplitude for non-resonant process depicted in Fig. 3(a) in the c.m. frame is obtained as

$$\mathcal{M}_{(a)} = -\frac{y_s}{\mu} \frac{Z_p}{M_p} I_{(a)}^{ij} \frac{e}{2} \chi_p^T \epsilon_\gamma^{*i} \sigma_2 \sigma_j \tau_2 \chi_N, \quad (24)$$

where $I_{(a)}^{ij}$ comes from the loop integration defined as

$$\begin{aligned}I_{(a)}^{ij} &= \int \frac{d^3\ell d^3\ell'}{(2\pi)^6} d^3r d^3r' d^3r'' \ell_i \ell'_j \langle \ell' | \mathbf{r}' \rangle \\ &\times \langle \mathbf{r}' | G_C(-B) | \mathbf{r} \rangle \left\langle \mathbf{r} \left| \boldsymbol{\ell} - \frac{\mu}{M_p} \mathbf{k} \right| \right\rangle \langle \ell | \mathbf{r}'' \rangle \langle \mathbf{r}'' | \psi_{\mathbf{p}} \rangle.\end{aligned}\quad (25)$$

Here, B is the binding energy of ^{16}O relative to the p - ^{15}N breakup threshold, \mathbf{k} is the outgoing photon momentum, and $\langle \mathbf{r} | \psi_{\mathbf{p}} \rangle = \psi_{\mathbf{p}}(\mathbf{r})$ is the Coulomb wave function. One can expand the Coulomb wave function and Green's function by partial waves as

$$\psi_{\mathbf{p}}(\mathbf{r}) = \sum_{l=0}^{\infty} (2l+1) i^l e^{i\sigma_l} P_l(\hat{\mathbf{r}} \cdot \hat{\mathbf{p}}) \frac{F_l(\eta, \rho)}{\rho}, \quad (26)$$

$$\langle \mathbf{r}' | G_C(E) | \mathbf{r} \rangle = \sum_{l=0}^{\infty} (2l+1) G_C^{(l)}(E; r', r) P_l(\hat{\mathbf{r}}' \cdot \hat{\mathbf{r}}), \quad (27)$$

where $\rho = pr$, $\sigma_l = \arg[\Gamma(l+1+i\eta)]$ is the Coulomb phase shift, $P_l(x)$ is the Legendre polynomial, and $F_l(\eta, \rho)$ is the regular Coulomb function. It can be easily verified that the s -wave ($l=0$) contribution in Eq. (27) vanishes by symmetry consideration and only the p -wave ($l=1$) part contributes. In

⁷ This is an expansion by p/κ and, since p of the second resonance region is close to the value of κ , the expansion would be questionable. In our case, however, the expansion of the function $\text{Re } H(\eta)$ converges fast and is valid within 5% even in the second resonance region ($E_{\text{cm}} \lesssim 1.5$ MeV).

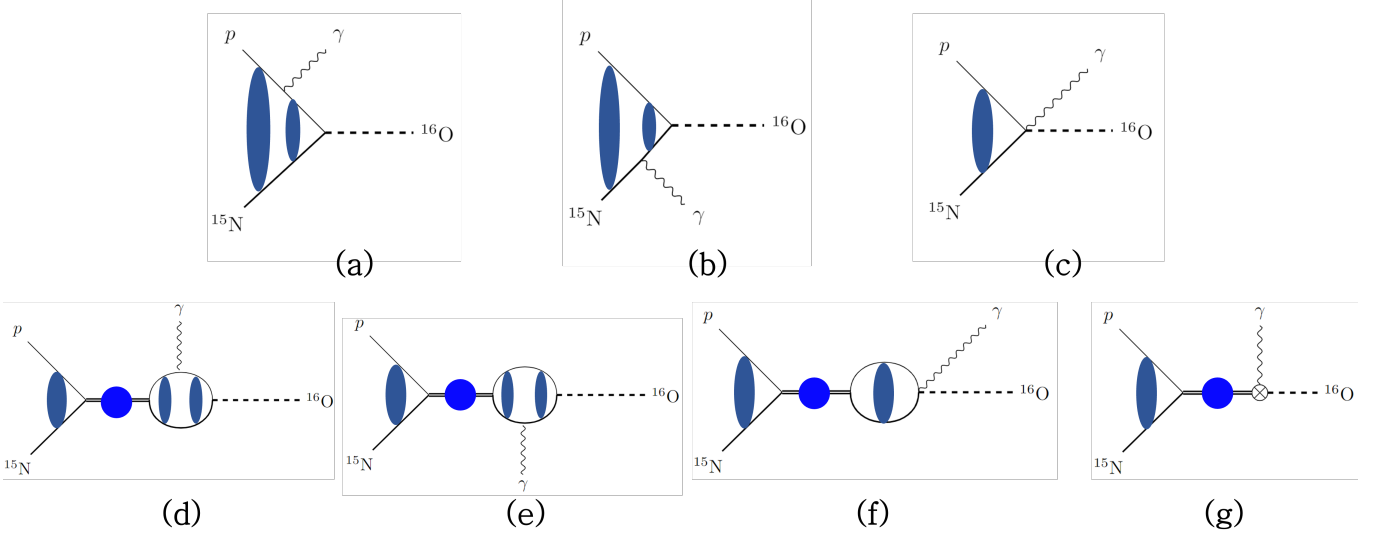


FIG. 3. Feynman diagrams for the radiative capture process of $^{15}\text{N}(p, \gamma)^{16}\text{O}$. The thin and thick solid lines denote the proton and the ^{15}N nucleus, respectively, and the wavy line stands for the out-going photon. The dotted line represents the ground state of the ^{16}O nucleus in the final state. The shaded blobs represent the Coulomb repulsion between the proton and ^{15}N . The circle with a cross in (g) is introduced as a counterterm of the loop diagrams.

Ref. [57], the partial-wave-expanded Coulomb Green's function $G_C^{(l)}$ for the bound state is shown to be simplified when it is written in terms of the regular and irregular Coulomb functions, $F_l(\eta, \rho)$ and $G_l(\eta, \rho)$, which leads to

$$G_C^{(l)}(-B, \rho', \rho) = -\frac{\mu p}{2\pi} \frac{F_l(\eta, \rho')}{\rho'} \frac{iF_l(\eta, \rho) + G_l(\eta, \rho)}{\rho}. \quad (28)$$

Using the identities of the Coulomb functions [58] the loop

integration $I_{(a)}^{ij}$ is rewritten as

$$I_{(a)}^{ij} = \delta_{ij} \frac{2\mu\gamma}{3} \Gamma(2 + \kappa/\gamma) e^{i\sigma_0} \times \int_0^\infty dr r W_{-\kappa/\gamma, 3/2}(2\gamma r) j_0\left(\frac{\mu}{M_p} kr\right) \frac{\partial}{\partial r} \left(\frac{F_0(\eta, pr)}{pr} \right), \quad (29)$$

where $j_l(z)$ and $W_{i\eta, l+1/2}(2i\rho)$ are the spherical Bessel function and the Whittaker W -function, respectively. Here, $\gamma = \sqrt{2\mu B}$ is the binding momentum determined by the binding energy B of ^{16}O relative to the p - ^{15}N threshold. Hence, the amplitude $\mathcal{M}_{(a)}$ is obtained as

$$\mathcal{M}_{(a)} = -y_s \frac{2\gamma Z_p}{3M_p} \Gamma(2 + \kappa/\gamma) e^{i\sigma_0} \times \int_0^\infty dr r W_{-\kappa/\gamma, 3/2}(2\gamma r) j_0\left(\frac{\mu}{M_p} kr\right) \frac{\partial}{\partial r} \left(\frac{F_0(\eta, pr)}{pr} \right) \times \chi_p^T \frac{e}{2} \sigma_2 (\boldsymbol{\epsilon}_\gamma^* \cdot \boldsymbol{\sigma}) \tau_2 \chi_N. \quad (30)$$

The rest of the amplitudes can be calculated in a similar way, and the isospin-dependent terms in Eq. (21) are obtained as

$$X_{(a+b)} = y_s \frac{2\gamma}{3} \Gamma(2 + \kappa/\gamma) e^{i\sigma_0} \times \int_0^\infty dr r W_{-\kappa/\gamma, 3/2}(2\gamma r) \left[\frac{Z_N}{M_N} j_0\left(\frac{\mu}{M_N} kr\right) - \frac{Z_p}{M_p} j_0\left(\frac{\mu}{M_p} kr\right) \right] \frac{\partial}{\partial r} \left(\frac{F_0(\eta, pr)}{pr} \right), \quad (31)$$

$$X_{(c)} = y_s \left(\frac{Z_N}{M_N} - \frac{Z_p}{M_p} \right) C_\eta e^{i\sigma_0}, \quad (32)$$

$$X_{(d+e)}^{(I)} = y_s \frac{2\gamma}{3} \Gamma(1 + i\eta) \Gamma(2 + \kappa/\gamma) \frac{C_\eta e^{i\sigma_0}}{K^{(I)}(p) - 2\kappa H(\eta)} \times \int_0^\infty dr r W_{-\kappa/\gamma, 3/2}(2\gamma r) \left[\frac{Z_N}{M_N} j_0\left(\frac{\mu}{M_N} kr\right) - \frac{Z_p}{M_p} j_0\left(\frac{\mu}{M_p} kr\right) \right] \frac{\partial}{\partial r} \left(\frac{W_{-i\eta, 1/2}(-2ipr)}{r} \right), \quad (33)$$

$$X_{(f)}^{(I)} = y_s \frac{C_\eta e^{i\sigma_0}}{K^{(I)}(p) - 2\kappa H(\eta)} \left(\frac{Z_N}{M_N} - \frac{Z_p}{M_p} \right) \left(2\kappa H(\eta) - \frac{2\pi}{\mu} J_0^{\text{div}} \right), \quad (34)$$

$$X_{(g)}^{(I)} = -h^{(I)} \frac{4\pi Z_O}{\mu} \frac{C_\eta e^{i\sigma_0}}{K^{(I)}(p) - 2\kappa H(\eta)}. \quad (35)$$

The integrals of Eq. (31) and Eq. (33) can be rewritten in terms of the confluent hypergeometric functions instead of the

Coulomb and Whittaker functions [58]. In order to perform numerical integration, we simplify these integrals as

$$L_{(a+b)}(p) = \int_0^\infty dr e^{(-\gamma+ip)r} r^3 U(2 + \kappa/\gamma, 4, 2\gamma r) \left[\frac{Z_N}{M_N} j_0\left(\frac{\mu}{M_N} kr\right) - \frac{Z_p}{M_p} j_0\left(\frac{\mu}{M_p} kr\right) \right] \times [M(1 + i\eta, 2, -2ipr) - (1 + i\eta)M(2 + i\eta, 3, -2ipr)], \quad (36)$$

$$L_{(d+e)}(p) = \int_{r_c}^\infty dr e^{(-\gamma+ip)r} r^3 U(2 + \kappa/\gamma, 4, 2\gamma r) \left[\frac{Z_N}{M_N} j_0\left(\frac{\mu}{M_N} kr\right) - \frac{Z_p}{M_p} j_0\left(\frac{\mu}{M_p} kr\right) \right] \times [U(1 + i\eta, 2, -2ipr) + 2(1 + i\eta)U(2 + i\eta, 3, -2ipr)], \quad (37)$$

so that $X_{(a+b)}$ and $X_{(d+e)}^{(I)}$ can be reexpressed as

$$X_{(a+b)} = i y_s \frac{8\gamma^3 p}{3} \Gamma(2 + \kappa/\gamma) C_\eta e^{i\sigma_0} L_{(a+b)}, \quad (38)$$

$$X_{(d+e)}^{(I)} = y_s \frac{16\gamma^3 p^2}{3} \Gamma(1 + i\eta) \Gamma(2 + \kappa/\gamma) \times \frac{C_\eta e^{i\sigma_0}}{K^{(I)}(p) - 2\kappa H(\eta)} L_{(d+e)}, \quad (39)$$

where $M(a, c, z)$ and $U(a, c, z)$ are the confluent hypergeometric functions of the first and second kinds, respectively. The detailed derivation is given in the Appendix.

The cut-off r_c is introduced in the integration of Eq. (37) to avoid divergence. The divergence from its rest part and the bubble diagram in Fig. 3(f) are absorbed by the counter term containing the LEC $h_R^{(I)}$, which is defined by

$$h_R^{(I)} = h^{(I)} + \frac{y_s}{Z_O} \left(\frac{Z_N}{M_N} - \frac{Z_p}{M_p} \right) \left(\frac{1}{2} J_0^{\text{div}} + L_{(d+e)}^{\text{div}} \right), \quad (40)$$

where J_0^{div} is given in Eq. (10) and $L_{(d+e)}^{\text{div}}$ is the divergence part coming from the loop in the diagram (d) and (e) in Fig. 3.

Explicitly, it reads

$$L_{(d+e)}^{\text{div}} = \frac{\mu}{6\pi} \int_0^{r_c} \frac{dr}{r^2} - \frac{\mu\kappa}{2\pi} \int_0^{r_c} \frac{dr}{r}, \quad (41)$$

which has both logarithmic and linear divergences. The dependence of the LECs and the astrophysical S factor on the cut-off value of r_c will be examined in the next section.

V. NUMERICAL RESULTS

The purpose of the present work is to extrapolate the astrophysical S factors, or equivalently the total cross sections, of the $^{15}\text{N}(p, \gamma)^{16}\text{O}$ reaction to the extremely low energy regions corresponding to stellar environments which are hard to reach in laboratory. The astrophysical S factor is defined by the total cross section $\sigma(E)$ that is given by

$$\sigma(E) = \frac{1}{4\pi} \frac{\gamma^2 + p^2}{4p} \sum_{\text{spins}} |\mathcal{M}|^2, \quad (42)$$

in the non-relativistic limit up to the leading terms in $1/M$ expansion [53], where \mathcal{M} is the capture amplitude defined

in Eq. (21), and γ and p are introduced in the previous section. Using the measured masses of the nuclei we obtain $\gamma \approx 146$ MeV.⁸

The effective Lagrangian (3) contains the following LECs: y_s , $y_t^{I=0,1}$, and $h_R^{I=0,1}$. In addition, since we include two s -wave resonance states of ^{16}O , one with $I = 0$ and the other with $I = 1$, by employing ERE, additional parameters for each resonance state are introduced as shown in Eq. (13). However, as Eq. (11) shows, the inverse of the squared $y_t^{I=0,1}$ is multiplied to the corresponding di-field propagator and this factor is canceled out when multiplied by the vertex functions. Therefore, these two LECs are redundant and cannot be determined through the analysis of the present work. The coupling constant y_s determines the strength of the coupling between the 3P_0 state of the p - ^{15}N system and the ground state of ^{16}O . The $h_R^{(I=0,1)}$ terms are the counter terms which absorb the divergences from the loop integrals and the values of $h_R^{(I=0,1)}$ depend on the cut-off r_c in Eq. (41). Furthermore, throughout numerical computations, we found that the ERE for the first resonance of iso-singlet gives stable results with the terms up to $O(p^2)$, while $O(p^6)$ expansion is needed for the second resonance of iso-triplet. These ERE parameters are rephrased in terms of the resonance energies (E_{R0} , E_{R1}), widths (Γ_{R0} , Γ_{R1}), and higher order corrections $R(E)$ for the second resonance, which introduces two parameters (a , b). As a result, we have totally 9 parameters, namely, y_s , $h^{I=0,1}$, E_{R0} , E_{R1} , Γ_{R0} , Γ_{R1} , a , and b on top of the cut-off r_c value.

In this study, we work with three different data sets reported by Refs. [11, 18, 25]. The old data set of Ref. [11], referred to as RR, contains 53 data points which cover the energy range of $150 \text{ keV} < E_p < 2500 \text{ keV}$. The 80 data points reported by Ref. [18], referred to as LeB, cover the energy range of $130 \text{ keV} < E_p < 1800 \text{ keV}$. The most recent data reported by Ref. [25], referred to as Imb, cover the similar energy region, $140 \text{ keV} < E_p < 1800 \text{ keV}$ with 78 data points.⁹ We use these data sets separately to determine our model parameters, which enables us to predict the astrophysical S factor at zero energy.

For the fitting process, we adopt the Markov chain Monte Carlo (MCMC) method [59] to minimize χ^2 defined as $\chi^2 = \sum_i (S_i^{\text{Theor.}} - S_i^{\text{Expt.}})^2 / (S_i^{\text{Err.}})^2$. Figure 4 presents our results for the astrophysical S factor of the $^{15}\text{N}(p,\gamma)^{16}\text{O}$ reaction as a function of the c.m. energy E . In Fig. 5, the same results are shown in logarithmic scales in both axes to highlight the extrapolated S factor in the very low energy region, which explicitly shows that the S factor becomes nearly flat as $E \rightarrow 0$. The bands in these figures indicate the errors in the S factor estimation of the MCMC calculations, which are estimated from the elements of the covariance matrix.

The fitted parameter values and the predicted $S(0)$ for the three data sets are given in Table I. This shows that the res-

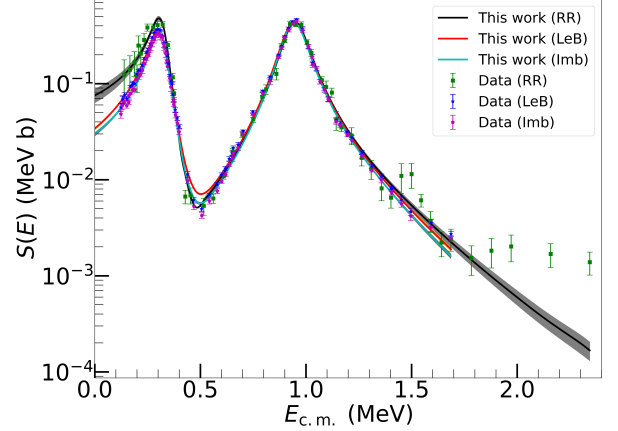


FIG. 4. The astrophysical S factor. The parameters are fitted by the three experimental data sets from Ref. [11] (RR), [18] (LeB), and [25] (Imb). The bands indicate the error range obtained in the MCMC calculations.

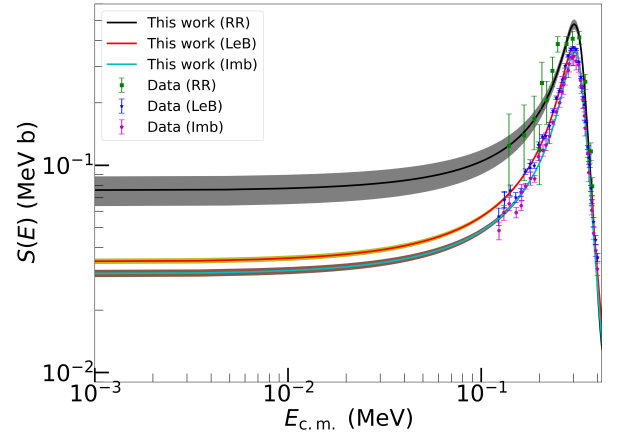


FIG. 5. Same as Fig. 4 but with logarithmic scales in both axes.

onance parameters are consistent to each other, which is expected as the three data sets share the same structure arising from the two resonances. The differences in the magnitudes, in particular, between the old [11] and new data [18, 25] are reflected mostly in the differences in the couplings y_s and $h_R^{I=0}$. This behavior is also understood as the gaps among data sets lie mostly in the very low energy region where the direct coupling (y_s) and the coupling to the iso-singlet resonance of ^{16}O ($h_R^{I=0}$) dominate.

The fitted resonance parameters are $E_{R0} \approx 360 - 370$ keV, $\Gamma_{R0} \approx 250 - 350$ keV, $E_{R1} \approx 960 - 970$ keV, and $\Gamma_{R1} \approx 155 - 160$ keV. These should be compared with the experimentally measured values of Ref. [60], namely, $E_{R0}^{\text{Expt.}} = 312$ keV, $\Gamma_{R0}^{\text{Expt.}} = 91$ keV, $E_{R1}^{\text{Expt.}} = 926$ keV, and $\Gamma_{R1}^{\text{Expt.}} = 130$ keV. We can see that the differences between resonance parameters in the present work and the empirical values are within

⁸ In the present work, we use $M_p = 938.272$ MeV for the proton mass, $M_N = 13968.936$ MeV for the ^{15}N mass, and $M_O = 14895.081$ MeV for the ^{16}O mass.

⁹ The data set of Ref. [18] was revised in Ref. [26]. We use the revised data set in the present work.

Data Set	y_s	$h_R^{(I=0)}$	$h_R^{(I=1)}$	E_{R0}	Γ_{R0}	E_{R1}	Γ_{R1}	a	b	χ^2/datum	$S(0)$	$S(E_G)$
RR [11]	2.759	3.410	-29.98	364.6	259.6	967.2	155.9	-0.389	1.158	2.43	75.3 ± 12.1	80.9 ± 12.5
LeB [18]	0.603	0.585	-31.46	369.3	347.4	962.9	160.0	-0.278	1.417	5.04	34.1 ± 0.9	38.2 ± 1.0
Imb [25]	0.897	0.978	-31.05	359.8	252.1	962.6	154.6	-0.326	1.636	2.58	29.8 ± 1.1	33.2 ± 1.1

TABLE I. The fitted values of the parameters for each data set and the derived astrophysical S factor at $E = 0$ and at the Gamow energy $E_G = 26$ keV. The units of y_s are $10^{-2} \text{ MeV}^{-1/2}$ and those of h_R^I are $10^{-3} \text{ MeV}^{1/2}$. The energies and widths of the resonances are given in the units of keV. The units of a and b are MeV^{-1} and MeV^{-2} , respectively, and the astrophysical S factors are in the units of keV b. For the cut-off value, we use $r_c = 1.0$ fm.

Data Set	RR [11]	LeB [18]	Imb [25]
$a_R^{(I=0)}$ (10^4 fm)	-1.722	-1.761	-1.824
$\tilde{r}^{(I=0)}$ (10^{-3} fm)	-7.053	-6.993	-6.746
$a_R^{(I=1)}$ (fm)	-21.44	-19.04	-18.87
$\tilde{r}^{(I=1)}$ (fm)	-4.342	-5.250	-5.319
$\tilde{P}^{(I=1)}$ (fm^3)	-144.07	-189.5	-192.6
$\tilde{Q}^{(I=1)}$ (fm^5)	-246.26	-339.5	-345.2
$r^{(I=0)}$ (fm)	1.457	1.457	1.458
$r^{(I=1)}$ (fm)	-2.878	-3.786	-3.855
$P^{(I=1)}$ (fm^3)	-149.72	-195.1	-198.2
$Q^{(I=1)}$ (fm^5)	-233.28	-326.5	-332.2

TABLE II. Reduced effective range parameters and effective range parameters for each data set.

5–20% except Γ_{R0} . Our fitted Γ_{R0} is more than three times the empirical value $\Gamma_{R0}^{\text{Expt.}}$. Such a difference is also seen in the $\alpha\alpha$ scattering study within EFT in Ref. [54]. Furthermore, the structures in the astrophysical S factors shown in Fig. 4 are reasonably reproduced by the present resonance parameters. In fact, our results indicate that the resonance structure in the astrophysical S factor is not sensitive to the value of Γ_{R0} , and, therefore, constraining the value of Γ_{R0} by this reaction is not easy.¹⁰ Thus the resolution of the difference in resonance parameters deserve more detailed and comprehensive studies [46].

As in R -matrix analyses [10, 11, 26], we find that there is a destructive interference between the two resonance contributions at $E \approx 0.5$ MeV, where the contributions from the two resonances overlap. We also find that the resonance contributions dominate the cross sections and the direct emission of the photon without a resonance shown in Figs. 3(a,b,c) is suppressed.

Shown in Table II are the effective range parameters and the reduced effective range parameters derived from the resonance parameters given in Table I. As we have seen above, all three data sets share the similar structures in the astrophysical S

$S(0)$ (keV b)	
Data of Ref. [10]	
Ref. [10]	32 ^a
Ref. [15]	35–40
Data of Ref. [11]	
Ref. [11]	64 ± 6
Ref. [15]	50
This work (RR)	75.3 ± 12.1
Data of Refs. [10, 11]	
Ref. [14]	36.0 ± 6
Ref. [16]	21.1
Data of Ref. [18]	
Ref. [18]	39.6 ± 2.6
Ref. [24]	33.1–40.1
Ref. [26]	40 ± 3
This work (LeB)	34.1 ± 0.9
Compiled data	
Ref. [22]	45^{+9}_{-7}
Ref. [27]	39.5–43.35 ^b
Data of Ref. [19]	
Ref. [47]	30.4
Data of Ref. [25]	
This work (Imb)	29.8 ± 1.1

^a This value is obtained for the proton energy of 25 keV in the laboratory frame, which gives the equivalent value of $S(0) \approx 26$ keV b [11].

^b The authors of Ref. [27] obtained these values for $E_p = 50$ –60 keV and accepted it as $S(0)$.

TABLE III. Estimated values of $S(0)$ for the $^{15}\text{N}(p, \gamma)^{16}\text{O}$ reaction in the units of keV b. The estimated values are categorized by the used data set(s).

factor coming from the resonances, and it is expected that they have similar ERE parameters. For the first resonance we take ERE up to $O(p^2)$ and for the second resonance we take up to $O(p^6)$. Our results show that the effects from the κ terms in the reduced effective range parameters are non-trivial, in particular, for the effective range \tilde{r} . We find that there is a big cancellation in $\tilde{r}^{(I=0)}$ between $r^{(I=0)}$ and the κ term, which leads to a fine tuning of the value of $\tilde{r}^{(I=0)}$.

¹⁰ The fitting was tried with forcing $\Gamma_{R0}^{\text{Expt.}} = 91$ keV. In this case, although the broadness of the curve of $S(E)$ in the first resonance region does not change, it overestimates the height of the resonance peak.

Since we have introduced the cut-off r_c in the loop integral, the results presented in the present work are obtained by taking $r_c = 1$ fm. In order to see the r_c -dependence of our results, we varied the values of r_c from 0.1 fm to 1.0 fm to confirm that the r_c -dependence of our results on the astrophysical S factor are very weak although the coupling strengths would change.

In Table III, we list the previous estimates of the astrophysical S factor at zero energy $S(0)$ from the R -matrix analysis [10, 11, 14, 15, 18, 24, 26] or potential model calculations [16, 22, 27]. Those values of $S(0)$ are scattered from 22 keV b to 64 keV b, depending on the data used for the fit. We first note that our estimate on the central value of the astrophysical $S(0)$ using the data of Ref. [11] is somehow larger than the values of the R matrix analyses of Refs. [11, 15] but the large error ranges overlap each other. However, these estimates differ from the $S(0)$ value extracted from the post-NACRE data of Refs. [18, 25], which give new values around 30 keV b. Our results are also close to the values extracted from the data sets up to the energy region of the first resonance reported in Refs. [22, 27, 47]. The comparison of our results for $S(0)$ with the values in the literature are visualized as well in Fig. 6. The results presented in Table III also shows that the S factor at the Gamow energy is about 10% larger than $S(0)$.

VI. SUMMARY AND DISCUSSION

In the present work, we studied the radiative proton capture process, $^{15}\text{N}(p,\gamma)^{16}\text{O}$, that has an important role in the CNO cycle by connecting the CN cycle and the NO cycle. Our study was performed by employing the EFT formalism, and, to our knowledge, there was no application of EFT approach for the investigation of this reaction. Three open channels of α - ^{12}C , α - $^{12}\text{C}^*$, and p - ^{15}N can be involved to describe the resonant states of ^{16}O , and the experimental data of the $^{15}\text{N}(p,\gamma)^{16}\text{O}$ reaction clearly show the structure of the two resonant 1^- states of $^{16}\text{O}^*$. One of them is the isospin singlet state and the other is the isospin triplet state, which have the excitation energies of 12.45 MeV and 13.09 MeV, respectively.

In order to describe this reaction, we employ a minimum set of effective Lagrangian with the terms for the two 1^- states with $I = 0$ and $I = 1$ in the p - ^{15}N channel. The resonances are described by the di-fields and the structure of their propagators are rephrased in terms of ERE and by taking the Breit-Wigner form. The parameters introduced in the low-energy effective Lagrangian are fitted to the available experimental data of the astrophysical S factor of the $^{15}\text{N}(p,\gamma)^{16}\text{O}$ reaction in the range of $E_p = 130$ keV to 2500 keV. In the present analysis, we employ the experimental data reported in Refs. [11, 18, 25] and the fitting process was performed for each data set using the MCMC method. Then the astrophysical S factors at $E = 0$ and $E = E_G$ are extrapolated and compared with the estimates in the literature. Our results show that the value of $S(0)$ is in the range of 30–35 keV b based on the data of Refs. [18, 25], which agrees with other estimates based on the post-NACRE data. We also found that the values of $S(E_G)$ are about 10% larger than those of $S(0)$.

The present work shows that the EFT approach can be ap-

plied to the study of $^{15}\text{N}(p,\gamma)^{16}\text{O}$. However, the extracted resonance parameters are puzzling as they show some discrepancies with the empirical values, in particular for the first resonance state although the resonance structures in the astrophysical S factor are well reproduced. The overestimate of a resonance width was also found in $\alpha\alpha$ scattering study within EFT, but the experimental value of a width of ^{16}O could be well reproduced in the study of the S factor of $^{12}\text{C}(\alpha,\gamma)^{16}\text{O}$ within EFT [29]. This deserves more detailed and rigorous investigations including the effects of other open channels.

ACKNOWLEDGMENTS

We are grateful to T.-S. H. Lee for fruitful discussions. This work was supported by the National Research Foundation of Korea (NRF) under Grants No. NRF-2019R1F1A1040362, No. NRF-2022R1F1A1070060, No. NRF-2020R1A2C1007597, and No. NRF-2018R1A6A1A06024970 (Basic Science Research Program).

Appendix: Loop integrals

In this Appendix, we derive the integrals of Eqs. (36) and (37) explicitly by using identities of the Coulomb functions, Whittaker functions, and the confluent hypergeometric functions [58]. The Coulomb function $F_l(\eta, \rho)$ is written as

$$F_l(\eta, \rho) = C_l(\eta)\rho^{l+1}e^{i\rho}M(l+1+i\eta, 2l+2, -2i\rho), \quad (\text{A.1})$$

where $M(a, c, z)$ is the confluent hypergeometric function of the first kind or the Kummer's function. The factor of $C_l(\eta)$ is defined as

$$C_l(\eta) = \frac{2^l}{(2l+1)!}|\Gamma(l+1+i\eta)|e^{-\frac{\pi}{2}\eta}, \quad (\text{A.2})$$

which becomes the Gamow factor for $l = 0$, namely, $C_0(\eta)$ becomes C_η of Eq. (15). On the other hand, the Whittaker function $W_{\kappa,\mu}(z)$ is written as

$$W_{\kappa,\mu}(z) = e^{-\frac{z}{2}}z^{\mu+\frac{1}{2}}U(\mu-\kappa+\frac{1}{2}, 1+2\mu, z), \quad (\text{A.3})$$

where $U(a, c, z)$ is the confluent hypergeometric function of the second kind or the Tricomi's function.

Using Eqs. (A.1) and (A.3), it is straightforward to get

$$W_{-\kappa/\gamma, 3/2}(2\gamma r) = 4\gamma^2 r^2 e^{-\gamma r} U(2+\kappa/\gamma, 4, 2\gamma r), \quad (\text{A.4})$$

$$\frac{W_{-i\eta, 1/2}(-2ipr)}{r} = -2ipe^{ipr} U(1+i\eta, 2, -2ipr), \quad (\text{A.5})$$

$$\frac{F_0(\eta, pr)}{pr} = C_\eta e^{ipr} M(1+i\eta, 2, -2ipr). \quad (\text{A.6})$$

As the loop integrals of Eqs. (31) and (33) contain derivatives of the above functions, we use the identities of the derivative of the confluent hypergeometric functions as

$$\frac{d}{dz}M(a, c, z) = \frac{a}{c}M(a+1, c+1, z), \quad (\text{A.7})$$

$$\frac{d}{dz}U(a, c, z) = -aU(a+1, c+1, z) \quad (\text{A.8})$$

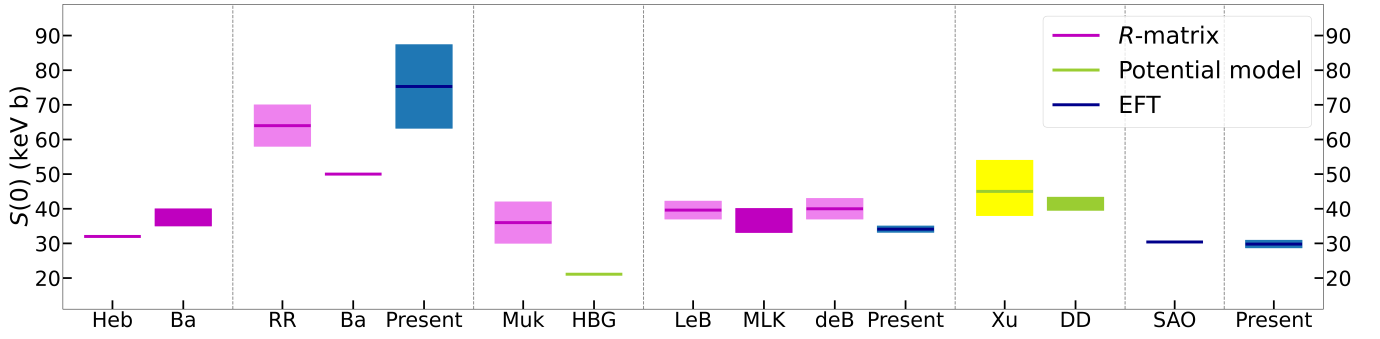


FIG. 6. The obtained $S(0)$ values of the present work compared with the values in the literature. The abbreviated references are as follows: Heb [10], Ba [15], RR [11], Muk [14], HBG [16], LeB [18], MLK [24], deB [26], Xu [22], DD [27], Caci [19], SAO [47], and Imb [25]. The references in the upper part indicate the sources of the experimental data and the references in the lower part indicate the sources of the calculated results.

to obtain the formulas of Eqs. (38) and (39). This finally leads to the integrals of Eqs. (31) and (33) in the simplified form of

$$\begin{aligned}
 & \int_0^\infty dr r W_{-\kappa/\gamma, 3/2}(2\gamma r) \left[\frac{Z_N}{M_N} j_0 \left(\frac{\mu}{M_N} kr \right) - \frac{Z_p}{M_p} j_0 \left(\frac{\mu}{M_p} kr \right) \right] \frac{\partial}{\partial r} \left(\frac{F_0(\eta, pr)}{pr} \right) \\
 &= 4\gamma^2 i p C_\eta \int_0^\infty dr e^{(-\gamma+ip)r} r^3 U(2+\kappa/\gamma, 4, 2\gamma r) \left[\frac{Z_N}{M_N} j_0 \left(\frac{\mu}{M_N} kr \right) - \frac{Z_p}{M_p} j_0 \left(\frac{\mu}{M_p} kr \right) \right] \\
 & \quad \times [M(1+i\eta, 2, -2ipr) - (1+i\eta)M(2+i\eta, 3, -2ipr)], \tag{A.9}
 \end{aligned}$$

and

$$\begin{aligned}
 & \int_0^\infty dr r W_{-\kappa/\gamma, 3/2}(2\gamma r) \left[\frac{Z_N}{M_N} j_0 \left(\frac{\mu}{M_N} kr \right) - \frac{Z_p}{M_p} j_0 \left(\frac{\mu}{M_p} kr \right) \right] \frac{\partial}{\partial r} \left(\frac{W_{-i\eta, 1/2}(-2ipr)}{r} \right) \\
 &= 8\gamma^2 p^2 \int_0^\infty dr e^{(-\gamma+ip)r} r^3 U(2+\kappa/\gamma, 4, 2\gamma r) \left[\frac{Z_N}{M_N} j_0 \left(\frac{\mu}{M_N} kr \right) - \frac{Z_p}{M_p} j_0 \left(\frac{\mu}{M_p} kr \right) \right] \\
 & \quad \times [U(1+i\eta, 2, -2ipr) + 2(1+i\eta)U(2+i\eta, 3, -2ipr)]. \tag{A.10}
 \end{aligned}$$

Embedding the cut-off r_c on the integration range of Eq. (A.10) gives Eqs. (38) and (39).

-
- [1] E. M. Burbidge, G. R. Burbidge, W. A. Fowler, and F. Hoyle, Synthesis of the elements in stars, *Rev. Mod. Phys.* **29**, 547 (1957).
 - [2] E. G. Adelberger *et al.*, Solar fusion cross sections. II. The pp chain and CNO cycles, *Rev. Mod. Phys.* **83**, 195 (2011).
 - [3] G. Bellini *et al.* (Borexino Collaboration), First Evidence of pep Solar Neutrinos by Direct Detection in Borexino, *Phys. Rev. Lett.* **108**, 051302 (2012).
 - [4] M. Agostini *et al.* (Borexino Collaboration), Comprehensive measurement of pp -chain solar neutrinos, *Nature* **562**, 505 (2018).
 - [5] M. Agostini *et al.* (Borexino Collaboration), Experimental evidence of neutrinos produced in the CNO fusion cycle in the Sun, *Nature* **587**, 577 (2020).
 - [6] G. D. O. Gann, K. Zuber, D. Bemmerer, and A. Serenelli, The future of solar neutrinos, *Annu. Rev. Nucl. Part. Sci.* **71**, 491 (2021).
 - [7] M. Wiescher, J. Görres, E. Uberseder, G. Imbriani, and M. Pig-natari, The cold and hot CNO cycles, *Annu. Rev. Nucl. Part. Sci.* **60**, 381 (2010).
 - [8] A. Boeltzig *et al.*, Shell and explosive hydrogen burning: Nuclear reaction rates for hydrogen burning in RGB, AGB and novae, *Eur. Phys. J. A* **52**, 75 (2016).
 - [9] J. José and M. Hernanz, Nucleosynthesis in classical novae: CO versus ONe white dwarfs, *Astrophys. J.* **494**, 680 (1998).
 - [10] D. F. Hebbard, Proton capture by ^{15}N , *Nucl. Phys.* **15**, 289 (1960).
 - [11] C. Rolfs and W. S. Rodney, Proton capture by ^{15}N at stellar energies, *Nucl. Phys.* **A235**, 450 (1974).
 - [12] A. Schardt, W. A. Fowler, and C. C. Lauritsen, The disintegration of N^{15} by protons, *Phys. Rev.* **86**, 527 (1952).
 - [13] F. Brochard, P. Chevallier, D. Disdier, V. Rauch, and F. Scheibling, Étude des désexcitations électromagnétiques des niveaux 1- situés à 12,44 et 13,09 MeV dans le noyau ^{16}O , *J. Phys.*

- France **34**, 363 (1973).
- [14] A. M. Mukhamedzhanov *et al.*, New astrophysical S factor for the $^{15}\text{N}(p, \gamma)^{16}\text{O}$ reaction via the asymptotic normalization coefficient (ANC) method, *Phys. Rev. C* **78**, 015804 (2008).
- [15] F. C. Barker, $^{15}\text{N}(p, \gamma_0)^{16}\text{O}$ S factor, *Phys. Rev. C* **78**, 044612 (2008).
- [16] J. T. Huang, C. A. Bertulani, and V. Guimarães, Radiative capture of nucleons at astrophysical energies with single-particle states, *Atom. Data Nucl. Data Tabl.* **96**, 824 (2010).
- [17] D. Bemmerer *et al.* (LUNA Collaboration), Direct measurement of the $^{15}\text{N}(p, \gamma)^{16}\text{O}$ total cross section at novae energies, *J. Phys. G* **36**, 045202 (2009).
- [18] P. J. LeBlanc *et al.*, Constraining the S factor of $^{15}\text{N}(p, \gamma)^{16}\text{O}$ at astrophysical energies, *Phys. Rev. C* **82**, 055804 (2010), *Phys. Rev. C* **84**, 019902(E) (2011).
- [19] A. Caciolli *et al.*, Revision of the $^{15}\text{N}(p, \gamma)^{16}\text{O}$ reaction rate and oxygen abundance in H-burning zones, *Astron. Astrophys.* **533**, A66 (2011).
- [20] A. Guglielmetti, Recent results on (p, γ) and (α, γ) fusion reactions at LUNA, *EPJ Web Conf.* **17**, 06001 (2011).
- [21] C. Broggini, D. Bemmerer, A. Caciolli, and D. Trezzi, LUNA: Status and prospects, *Prog. Part. Nucl. Phys.* **98**, 55 (2018).
- [22] Y. Xu, K. Takahashi, S. Goriely, M. Arnould, M. Ohta, and H. Utsunomiya, NACRE II: An update of the NACRE compilation of charged-particle-induced thermonuclear reaction rates for nuclei with mass number $A < 16$, *Nucl. Phys. A* **918**, 61 (2013).
- [23] Experimental Nuclear Reaction Data (EXFOR), <https://www-nds.iaea.org/nrdc/about/about-exfor.html>.
- [24] A. M. Mukhamedzhanov, M. La Cognata, and V. Kroha, Astrophysical S factor for the $^{15}\text{N}(p, \gamma)^{16}\text{O}$ reaction, *Phys. Rev. C* **83**, 044604 (2011).
- [25] G. Imbriani *et al.*, Measurement of γ rays from $^{15}\text{N}(p, \gamma)^{16}\text{O}$ cascade and $^{15}\text{N}(p, \alpha_1 \gamma)^{12}\text{C}$ reactions, *Phys. Rev. C* **85**, 065810 (2012), **86**, 039902(E) (2012).
- [26] R. J. deBoer, J. Görres, G. Imbriani, P. J. LeBlanc, E. Uberseder, and M. Wiescher, R -matrix analysis of ^{16}O compound nucleus reactions, *Phys. Rev. C* **87**, 015802 (2013).
- [27] S. Dubovichenko and A. Dzhezairov-Kakhramanov, Study of the neutron and proton capture reactions $^{10,11}\text{B}(n, \gamma)$, $^{11}\text{B}(p, \gamma)$, $^{14}\text{C}(p, \gamma)$, and $^{15}\text{N}(p, \gamma)$ at thermal and astrophysical energies, *Int. J. Mod. Phys. E* **23**, 1430012 (2014).
- [28] S. Weinberg, Phenomenological Lagrangians, *Physica* **96A**, 327 (1979).
- [29] S.-I. Ando, S_{E1} factor of radiative α capture on ^{12}C in cluster effective field theory, *Phys. Rev. C* **100**, 015807 (2019).
- [30] M. M. Khansari, H. Khalili, and H. Sadeghi, Cross section and astrophysical S -factor for $^{12}\text{C}(p, \gamma)^{13}\text{N}^*$ reaction with halo effective field theory at low-energies, *New Astron.* **57**, 76 (2017).
- [31] X. Zhang, K. M. Nollett, and D. R. Phillips, Combining *ab initio* calculations and low-energy effective field theory for halo nuclear systems: The case of $^7\text{Li} + n \rightarrow ^8\text{Li} + \gamma$, *Phys. Rev. C* **89**, 024613 (2014).
- [32] X. Zhang, K. M. Nollett, and D. R. Phillips, Halo effective field theory constrains the solar $^7\text{Be} + p \rightarrow ^8\text{B} + \gamma$ rate, *Phys. Lett. B* **751**, 535 (2015).
- [33] X. Zhang, K. M. Nollett, and D. R. Phillips, Models, measurements, and effective field theory: Proton capture on ^7Be at next-to-leading order, *Phys. Rev. C* **98**, 034616 (2018).
- [34] G. Rupak and R. Higa, Model-Independent Calculation of Radiative Neutron Capture on Lithium-7, *Phys. Rev. Lett.* **106**, 222501 (2011).
- [35] R. Higa, G. Rupak, and A. Vaghani, Radiative $^3\text{He}(\alpha, \gamma)^7\text{Be}$ reaction in halo effective field theory, *Eur. Phys. J. A* **54**, 89 (2018).
- [36] L. Moschini, J. Yang, and P. Capel, ^{15}C : From halo effective field theory structure to the study of transfer, breakup, and radiative-capture reactions, *Phys. Rev. C* **100**, 044615 (2019).
- [37] S.-I. Ando, Elastic α - ^{12}C scattering at low energies in cluster effective field theory, *Eur. Phys. J. A* **52**, 130 (2016).
- [38] S.-I. Ando, Elastic α - ^{12}C scattering at low energies with the bound states of ^{16}O in effective field theory, *Phys. Rev. C* **97**, 014604 (2018).
- [39] S.-I. Ando, Elastic α - ^{12}C scattering at low energies with the resonant 2_2^+ and 2_3^+ states of ^{16}O , [arXiv:2108.02386](https://arxiv.org/abs/2108.02386).
- [40] S.-I. Ando, Cluster effective field theory and nuclear reactions, *Eur. Phys. J. A* **57**, 17 (2021).
- [41] P. F. Bedaque and U. van Kolck, Effective field theory for few nucleon systems, *Annu. Rev. Nucl. Part. Sci.* **52**, 339 (2002).
- [42] G. Rupak, Radiative reactions in halo effective field theory, *Int. J. Mod. Phys. E* **25**, 1641004 (2016).
- [43] H.-W. Hammer, C. Ji, and D. R. Phillips, Effective field theory description of halo nuclei, *J. Phys. G* **44**, 103002 (2017).
- [44] P. Capel, Combining halo-EFT descriptions of nuclei and precise models of nuclear reactions, *Few-Body Syst.* **63**, 14 (2022).
- [45] B. A. Gelman, Narrow resonances and short-range interactions, *Phys. Rev. C* **80**, 034005 (2009).
- [46] J. B. Habashi, S. Fleming, and U. van Kolck, Nonrelativistic effective field theory with a resonance field, *Eur. Phys. J. A* **57**, 169 (2021).
- [47] S. Son, S.-I. Ando, and Y. Oh, Determination of astrophysical S factor for $^{15}\text{N}(p, \gamma)^{16}\text{O}$ at low-energies within effective field theory, *New Phys.: Sae Mulli* **72**, 291 (2022).
- [48] C. A. Bertulani, H.-W. Hammer, and U. van Kolck, Effective field theory for halo nuclei: shallow p -wave states, *Nucl. Phys. A* **712**, 37 (2002).
- [49] P. F. Bedaque, H.-W. Hammer, and U. van Kolck, Narrow resonances in effective field theory, *Phys. Lett. B* **569**, 159 (2003).
- [50] X. Kong and F. Ravndal, Proton-proton scattering lengths from effective field theory, *Phys. Lett. B* **450**, 320 (1999), **458**, 565(E) (1999).
- [51] X. Kong and F. Ravndal, Coulomb effects in low energy proton-proton scattering, *Nucl. Phys. A* **665**, 137 (2000).
- [52] D. B. Kaplan, M. J. Savage, and M. B. Wise, A new expansion for nucleon-nucleon interactions, *Phys. Lett. B* **424**, 390 (1998).
- [53] S.-I. Ando and C. H. Hyun, Effective field theory on the deuteron with dibaryon field, *Phys. Rev. C* **72**, 014008 (2005).
- [54] R. Higa, H.-W. Hammer, and U. van Kolck, $\alpha\alpha$ scattering in halo effective field theory, *Nucl. Phys. A* **809**, 171 (2008).
- [55] S.-I. Ando, Elastic α - ^{12}C scattering at low energies with the sharp resonant 0_3^+ state of ^{16}O , *Phys. Rev. C* **102**, 034611 (2020).
- [56] E. Ryberg, C. Forssén, H.-W. Hammer, and L. Platter, Effective field theory for proton halo nuclei, *Phys. Rev. C* **89**, 014325 (2014).
- [57] E. Ryberg, C. Forssén, H.-W. Hammer, and L. Platter, Constraining low-energy proton capture on beryllium-7 through charge radius measurements, *Eur. Phys. J. A* **50**, 170 (2014).
- [58] F. W. J. Olver, D. W. Lozier, R. F. Boisvert, and C. W. Clark, editors, *NIST Handbook of Mathematical Functions* (Cambridge University Press, 2010).
- [59] D. Foreman-Mackey, D. W. Hogg, D. Lang, and J. Goodman, emcee: The MCMC hammer, *PASP* **125**, 306 (2013).
- [60] D. R. Tilley, H. R. Weller, and C. M. Cheves, Energy levels of light nuclei $A = 16$ –17, *Nucl. Phys. A* **564**, 1 (1993).